Josephson oscillation and transition to self-trapping for Bose-Einstein condensates in a triple-well trap

Bin Liu,[1,2] Li-Bin Fu,[2] Shi-Ping Yang,[1] and Jie Liu[2,*]

[1]*College of Physics and Information Engineering, Hebei Normal University, 050016 Shijiazhuang, China*
[2]*Institute of Applied Physics and Computational Mathematics, P.O. Box 8009 (28), 100088 Beijing, China*
(Received 8 October 2006; published 2 March 2007)

We investigate the tunneling dynamics of Bose-Einstein condensates (BECs) in a symmetric as well as in a tilted triple-well trap within the framework of mean-field treatment. The eigenenergies as the functions of the zero-point energy difference between the tilted wells show a striking entangled star structure when the atomic interaction is large. We then achieve insight into the oscillation solutions around the corresponding eigenstates and observe several new types of Josephson oscillations. With increasing the atomic interaction, the Josephson-type oscillation is blocked and the self-trapping solution emerges. The condensates are self-trapped either in one well or in two wells but no scaling law is observed near transition points. In particular, we find that the transition from the Josephson-type oscillation to the self-trapping is accompanied with some irregular regime where tunneling dynamics is dominated by chaos. The above analysis is facilitated with the help of the Poincaré section method that visualizes the motions of BECs in a reduced phase plane.

I. INTRODUCTION

The first realization of dilute degenerate atomic gases in 1965 launched a new epoch for studying the dynamical property of Bose-Einstein condensates (BECs) [1]. For the dilute degenerate gases, essential dynamical property is included in the Gross-Pitaevskii equation (GPE) [2]. The nonlinearity, originated from the interatomic interaction, is included in the equation through a mean-field term proportional to condensate density. Previously, several authors investigated the dynamics of GPE for a double-well potential in a two-mode approximation [3–9]. Different features were found, e.g., the emergence of different nonlinear stationary states [5] and a variety of different crossing scenarios [9], nonzero adiabatic tunneling probability [4,7], etc., to name only a few. Among these findings, nonlinear Josephson oscillation and self-trapping phenomena are of most interest. As well be known, for a single particle in a symmetric double well, the tunneling dynamics is determined by the tunnelling splitting of two nearly degenerate eigenstates and tunneling time or quantum oscillation period is inversely proportional to the energy splitting [10]. When atomic interaction emerges, the tunneling between two wells is also observed, termed as nonlinear Josephson oscillation [3,6,8]. However, in this case, the oscillation period sensitively depends on the initial state but has little relation to the difference between the eigenenergies. More interestingly, increasing the atomic interaction further (even if it is repulsive), the Josephson oscillation between two wells is completely blocked, the BEC atoms in a symmetric double-well potential show a highly asymmetric distribution as if most atoms are trapped in one well [3]. This somehow counterintuitive phenomenon is termed as self-trapping and has been observed in the lab recently [11]. Recently, much attention has been paid to a trimer chain of BECs with periodic boundary condition, where self-trapping

mechanism [12], chaotic behavior and collective modes [13], and instability [14] have been investigated comprehensively.

In the present paper, we extend our investigation into tunneling dynamics for BECs in a triple-well system [15] (schematically sketched as in Fig. 1) and want to know how the nonlinear Josephson oscillation and self-trapping behave in this simplest multiwell system. Because quantum tunneling may happen between several wells simultaneously, we expect that the tunneling dynamics in the triple well will show more interesting behavior. Moreover, the study of the triple-well system will provide a bridge between the simple double well and the multiwell systems, helping us understand the "self-localized" phenomenon of BECs in the optical lattice [16].

Technically, to investigate the dynamics of triple-well systems we resort to the Poincaré section method [17] that visualizes the motion of BECs in a reduced two-dimensional phase plane. For our triple-well system, ignoring a total phase, the dynamics is governed by a Hamiltonian with two freedoms. Its phase space is four-dimensional. However, the motions in a high-dimensional phase space (in our case, it is 4D) are difficult to trace. With using the Poincaré section, we can investigate the motions of BEC in a reduced 2D phase plane.

Our paper is organized as follows. In Sec. II we introduce our model and show the unusual structure of the eigenenergies. In Sec. III we investigate nonlinear Josephson oscillations using the Poincaré section method and demonstrate di-
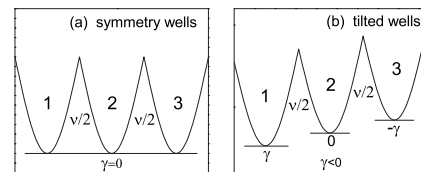

FIG. 1. The schematic sketch of our model. (a) The symmetric case ($\gamma=0$) and (b) the asymmetric case ($\gamma, 0, -\gamma$) is the zero-point energy in each well, respectively.

*Electronic address: Liu_Jie@iapcm.ac.cn

verse types of oscillations for BECs. In Sec. IV we investigate the transition from the Josephson oscillation to self-trapping of BECs in one well as well as in two wells and show an irregular regime characterized by chaos. Our discussions are extended to a tilted triple-well system in Sec. V. Section VI is our conclusions.

II. MODEL

For the triple-well system and under mean-field approximation, the wave function $\Psi(r,t)$ of GPE is the superposition of three wave functions describing the condensate in each trap, i.e.,

$$\Psi(r,t) = a_1(t)\phi_1(r) + a_2(t)\phi_2(r) + a_3(t)\phi_3(r). \quad (1)$$

Then the triple-well system is described by a dimensionless Schrödinger equation,

$$i\frac{d}{dt}\begin{pmatrix} a_1 \\ a_2 \\ a_3 \end{pmatrix} = \hat{H}\begin{pmatrix} a_1 \\ a_2 \\ a_3 \end{pmatrix}, \quad (2)$$

with the Hamiltonian

$$\hat{H} = \begin{pmatrix} \gamma + c|a_1|^2 & -\dfrac{v}{2} & 0 \\[2ex] -\dfrac{v}{2} & c|a_2|^2 & -\dfrac{v}{2} \\[2ex] 0 & -\dfrac{v}{2} & -\gamma + c|a_3|^2 \end{pmatrix}. \quad (3)$$

The total probability $|a_1|^2 + |a_2|^2 + |a_3|^2$ is conserved and is set to be a unit. c is the mean-field parameter denoting the atomic interaction, v is the coupling parameter, and γ is the zero-point energy of the wells. The schematic sketch of the model is shown in Fig. 1. In our following discussions, we focus on the case of repulsive interaction between atoms, i.e., $c > 0$.

The above Hamiltonian for the triple-well model is distinct from that of the trimer train model [12–14] in that the farmost off-diagonal terms vanish. Physically, the trimer train model is a periodic boundary condition or ring configuration, whereas the triple-well model is not. This leads to very different physics even in the linear case. For example, the ground state of the trimer train [13] corresponds to an equal distribution of the BEC population in each well. However, in the triple-well case, the ground state is of unbalanced population distribution, i.e., $(1/4, 1/2, 1/4)$ in the linear case. Moreover, there are no vortexlike, dimerlike configurations in the triple-well model but they do exists in the trimer train model. The fixed points and their properties are essentially different between the two systems.

Ignoring a total phase, the dynamics of the above three-level quantum system can be depicted by a classical Hamiltonian of two-degree freedom [15]. Let us show that $n_1 = |a_1|^2, n_2 = |a_2|^2, n_3 = |a_3|^2, \theta_1 = \arg a_1 - \arg a_2, \theta_3 = \arg a_3 - \arg a_2$, using the constraint $n_1 + n_2 + n_3 = 1$, we can get the classical Josephson Hamiltonian,
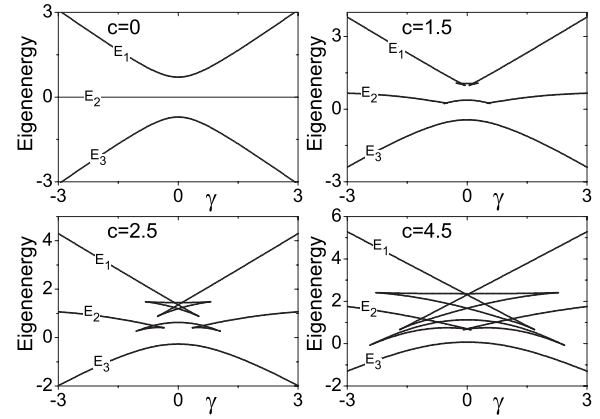

FIG. 2. The eigenenergy levels for different interaction strength. We have set $v = 1$.

$$\mathcal{H} = \gamma(n_1 - n_3) + \frac{1}{2}c[n_1^2 + n_3^2 + (1 - n_1 - n_3)^2]$$
$$- v\sqrt{1 - n_1 - n_3}(\sqrt{n_1}\cos\theta_1 + \sqrt{n_3}\cos\theta_3), \quad (4)$$

and the corresponding canonical equations,

$$\frac{dn_1}{dt} = -v\sin(\theta_1)\sqrt{n_1}\sqrt{1 - n_1 - n_3}, \quad (5a)$$

$$\frac{d\theta_1}{dt} = \gamma + \frac{1}{2}c[2n_1 - 2(1 - n_1 - n_3)] - \frac{v\cos(\theta_1)\sqrt{1 - n_1 - n_3}}{2\sqrt{n_1}}$$
$$+ \frac{v[\sqrt{n_1}\cos(\theta_1) + \cos(\theta_3)\sqrt{n_3}]}{2\sqrt{1 - n_1 - n_3}}, \quad (5b)$$

$$\frac{dn_3}{dt} = -v\sin(\theta_3)\sqrt{1 - n_1 - n_3}\sqrt{n_3}, \quad (5c)$$

$$\frac{d\theta_3}{dt} = -\gamma + \frac{1}{2}c[2n_3 - 2(1 - n_1 - n_3)]$$
$$+ \frac{v[\sqrt{n_1}\cos(\theta_1) + \cos(\theta_3)\sqrt{n_3}]}{2\sqrt{1 - n_1 - n_3}}$$
$$- \frac{v\cos(\theta_3)\sqrt{1 - n_1 - n_3}}{2\sqrt{n_3}}. \quad (5d)$$

The fixed point or minimum energy point of the classical Hamiltonian system (4) corresponds to the eigenstate of the quantum system [7,18]. To derive the analytical expressions of these fixed points is difficult, however, numerically, we can readily obtain them exploiting the MATHEMATICA software [19]. We plot the eigenenergies as the function of the zero-point energy bias in Fig. 2. They show unusual entangled star structure for the strong nonlinearity.

For the weak interactions, the eigenenergy levels are very similar to the linear case ($c = 0$). With an increase in nonlinearity (i.e., $c = 1.5$), the topological structure of the upper level changes: two small loops emerge. When the interaction is stronger (i.e., $c = 2.5$), the two loops will collide and form
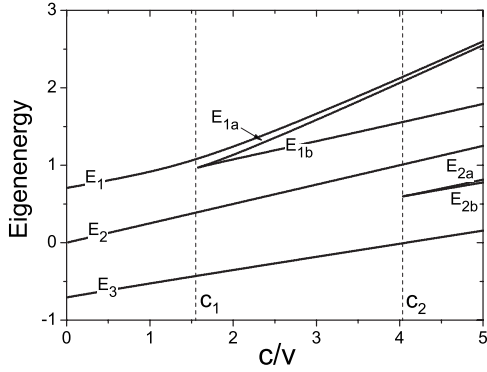
FIG. 3. When $\gamma=0$, the energy levels vary with the interaction strength c/v, where we set $v=1$.

a star structure, and then two more loops will emerge at the middle level E_2. For still stronger interaction (i.e., $c=4.5$), the star structure of the upper level entangles with the star structure in the lower level. However, we can still distinguish these levels because they have different relative phases. In fact, levels labeled by E_1 have relative phases $(\theta_1=\pi, \theta_3=\pi)$, levels labeled by E_2 have relative phases $(\theta_1=\pi, \theta_3=0)$ or $(\theta_1=0, \theta_3=\pi)$, and levels labeled by E_3 have relative phases $(\theta_1=0, \theta_3=0)$.

The relation between the chemical potential and the above energy is

$$E = \mu - \frac{c}{2}(|a_1|^4 + |a_2|^4 + |a_3|^4), \qquad (6)$$

where μ denotes the chemical potential defined as $\langle\Psi|H|\Psi\rangle$.

In the above calculations and henceforth, for convenience we set the coupling parameter as a unit, i.e., $v=1$.

III. SYMMETRIC TRIPLE-TRAP CASE, $\gamma=0$

Firstly we focus on the symmetric case, i.e., $\gamma=0$. The dependence of the energy levels on the interaction strength is exposed by Fig. 3. For the interaction strength less than a critical value $c_1=1.56$, the level structure is similar to its linear counterpart except for some positive shifts on the energy values. For $c > c_1$, two more levels labeled as (E_{1a}, E_{1b}) emerge. Actually, they correspond to the star structure of the upper level E_1 in Fig. 2 and have relative phases of $(\theta_1=\pi, \theta_3=\pi)$. When the interaction strength is still stronger and exceeds the second critical value $c_2=4.06$, two more energy levels labeled as (E_{2a}, E_{2b}) emerge. They correspond to the star structure of mid-level E_2 in Fig. 2 and have the same relative phases as that of E_2.

The stability of the corresponding eigenstates can be evaluated by the eigenvalues of the Jacobian of the classical Josephson Hamiltonian (4),

$$\mathcal{J} = \begin{pmatrix} -\dfrac{\partial^2 \mathcal{H}}{\partial n_1 \partial \theta_1} & -\dfrac{\partial^2 \mathcal{H}}{\partial \theta_1^2} & -\dfrac{\partial^2 \mathcal{H}}{\partial n_3 \partial \theta_1} & -\dfrac{\partial^2 \mathcal{H}}{\partial \theta_3 \partial \theta_1} \\[2mm] \dfrac{\partial^2 \mathcal{H}}{\partial n_1^2} & \dfrac{\partial^2 \mathcal{H}}{\partial \theta_1 \partial n_1} & \dfrac{\partial^2 \mathcal{H}}{\partial n_3 \partial n_1} & \dfrac{\partial^2 \mathcal{H}}{\partial \theta_3 \partial n_1} \\[2mm] -\dfrac{\partial^2 \mathcal{H}}{\partial n_1 \partial \theta_3} & -\dfrac{\partial^2 \mathcal{H}}{\partial \theta_1 \partial \theta_3} & -\dfrac{\partial^2 \mathcal{H}}{\partial n_3 \partial \theta_3} & -\dfrac{\partial^2 \mathcal{H}}{\partial \theta_3^2} \\[2mm] \dfrac{\partial^2 \mathcal{H}}{\partial n_1 \partial n_3} & \dfrac{\partial^2 \mathcal{H}}{\partial \theta_1 \partial n_3} & \dfrac{\partial^2 \mathcal{H}}{\partial n_3^2} & \dfrac{\partial^2 \mathcal{H}}{\partial \theta_3 \partial n_3} \end{pmatrix}. \qquad (7)$$

The eigenvalues of the above Jacobian have their correspondence of the Bogoliubov excitation spectrum of BECs. Pure imaginary values indicates a stable BEC state, whereas the emergence of real values implies instability for BECs and leads to a rapid production of the Bogoliubov quasiparticles [20]. From calculating the above Jacobian matrix and making the diagonalization, we know that the states corresponding to level E_{1b} and level E_{2b} are unstable and the others are stable.

A. Linear Josephson oscillation solution

For the linear Josephson oscillation, i.e., $c=0$, the system is analytically solvable. The solutions of (a_1, a_2, a_3) are

$$a_1 = C_2 \cos\left(\frac{v}{\sqrt{2}}t + C_3\right) + C_1, \qquad (8a)$$

$$a_2 = C_4 \cos\left(\frac{v}{\sqrt{2}}t + C_5\right), \qquad (8b)$$

$$a_3 = -\left\{C_2 \cos\left[\frac{v}{\sqrt{2}}\left(t + \frac{T}{2}\right) + C_3\right] + C_1\right\}, \qquad (8c)$$

where C_i are parameters determined by the initial conditions

$$C_2 \cos C_3 + C_1 = a_1(0), \qquad (9a)$$

$$C_4 \cos C_5 = a_2(0), \qquad (9b)$$

$$C_2 \cos C_3 - C_1 = a_3(0), \qquad (9c)$$

$$-\frac{v}{\sqrt{2}}C_2 \sin C_3 = i\frac{v}{2}a_2(0), \qquad (9d)$$

$$-\frac{v}{\sqrt{2}}C_4 \sin C_5 = i\frac{v}{2}[a_1(0) + a_3(0)], \qquad (9e)$$

and the constraint

$$|a_1(0)|^2 + |a_2(0)|^2 + |a_3(0)|^2 = 1. \qquad (10)$$

From the above explicit expressions, we see that a_1, a_2, and a_3 vary with respect to time periodically. They share a common period that is inversely proportional to the coupling parameter, i.e., $T = 2\sqrt{2}\pi/v$. Actually, the frequency is just
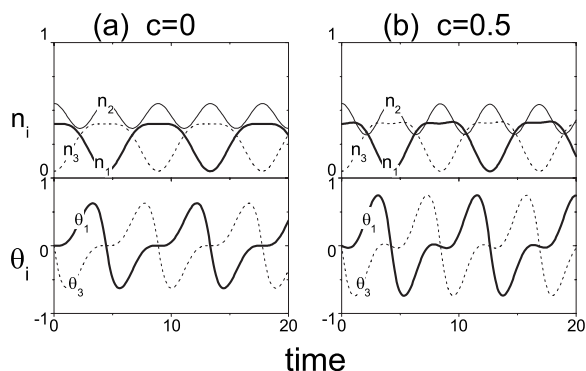
FIG. 4. The evolutions of n_1 (heavy line), n_2 (thin line), n_3 (dashed line) and θ_1 (heavy line), θ_3 (dashed line) in symmetric wells for the linear case (a) and the weak interactions case (b), with the same initial values ($n_1=0.4, n_3=0.05, \theta_1=0, \theta_3=0$).

the bias between eigenenergy levels. With initial conditions, the coefficients C_i will be fixed by using Eq. (9). In our case, $C_1 \neq 0$, so the period of population n_1 and n_3 is twice the period of n_2, and compared with n_1, variable n_3 has a phase delay of a half period. The above analysis is confirmed by our numerical simulations as shown in Fig. 4(a).

B. Weak interaction cases, $c < c_1$

The dynamics of this two-freedom system could be visualized from the Poincaré section [17]. We do this by solving the canonical equation (5d) numerically and then plotting θ_1 and n_1 at each time that $\theta_2=0$ and $\theta_2<0$. Notice the total energy is conserved, therefore the Poincaré sections consist of a picture panel where each picture corresponds to a fixed energy.

For the linear case, all motions share a common period exactly, and the Poincaré section is some isolated points. With weak interactions, the periodicity will be destroyed, and the motions become periodic or quasiperiodic, corresponding to the Poincaré section plotted in Fig. 5, where we see the section plane is full of stable islands. However, in this case the motion is similar to the linear case if they have the same initial values, as shown in Figs. 4(a) and 4(b).

C. Strong interaction cases, $c > c_2$

When the interaction is strong, the nonlinear effect is dominant. Accordingly, the Poincaré section is complicated,
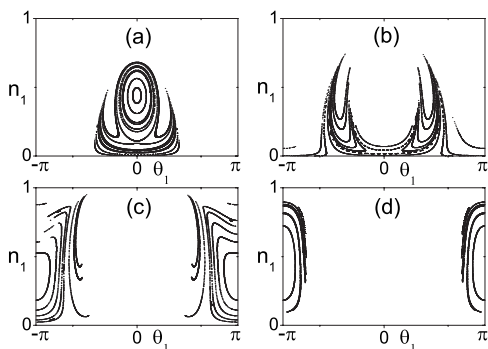

FIG. 5. The Poincaré section at $\theta_3=0$ for $c/v=0.5$ with different energy E. (a) $E=-0.4$, (b) $E=-0.1$, (c) $E=0.2$, (d) $E=0.5$.
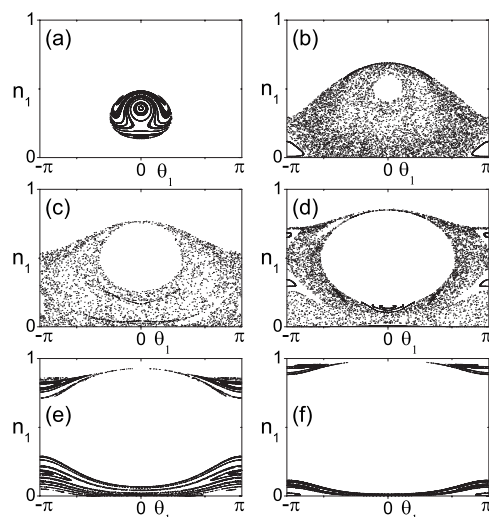

FIG. 6. The Poincaré section at $\theta_3=0$ for $c/v=5$ with different energy E. (a) $E=0.3$. (b) $E=0.8$. (c) $E=1.1$. (d) $E=1.5$. (e) $E=1.9$. (f) $E=2.3$.

as shown in Fig. 6, where we see many chaotic regions except for some stable islands. In the islands, the motions are periodic or quasiperiodic whereas in the chaotic region the motions are irregular. In order to grasp the dynamical property in this situation, we have simulated the motions for every regular island numerically, and find that except for the oscillations like the linear or weak interaction case, as shown in Fig. 7(a), there are also four types of new oscillations, as shown in Figs. 7(b)–7(e), respectively.

Figure 7(a) shows that the oscillation in well one is almost the same as that of well three except a phase delay of a half period. In order to compare with the linear or weak interaction case, we take the same initial value as that of Fig. 4. We see that their oscillations behavior is similar.

In addition to the case shown in Fig. 7(a), the motions of BECs in the triple well can demonstrate very different behavior. Figure 7(b) shows that almost all of the BEC atoms oscillate with small amplitude in two adjacent wells, i.e., well one and well two. The phase θ_1 oscillates around 0 and the phase θ_3 oscillates around π. The energy of these oscillations is closed to the eigenenergy of the level labeled by E_{2a}, and the center they surrounded is near the fixed point corresponding to level E_{2a}. As mentioned before, this fixed point is a stable point.

Figure 7(c) shows that almost all of the BEC atoms oscillate with large amplitude in well one and well two, and the relative phase θ_1 is always oscillating around zero. These oscillations are regarded as oscillations in a reduced two-well trapped system. In fact, because n_3 is small and c/v is very large, we can regard the term

$$H_1 = v\sqrt{1-n_1-n_3}\sqrt{n_3}\cos(\theta_3) \qquad (11)$$

as a perturbation. Using the generating function,

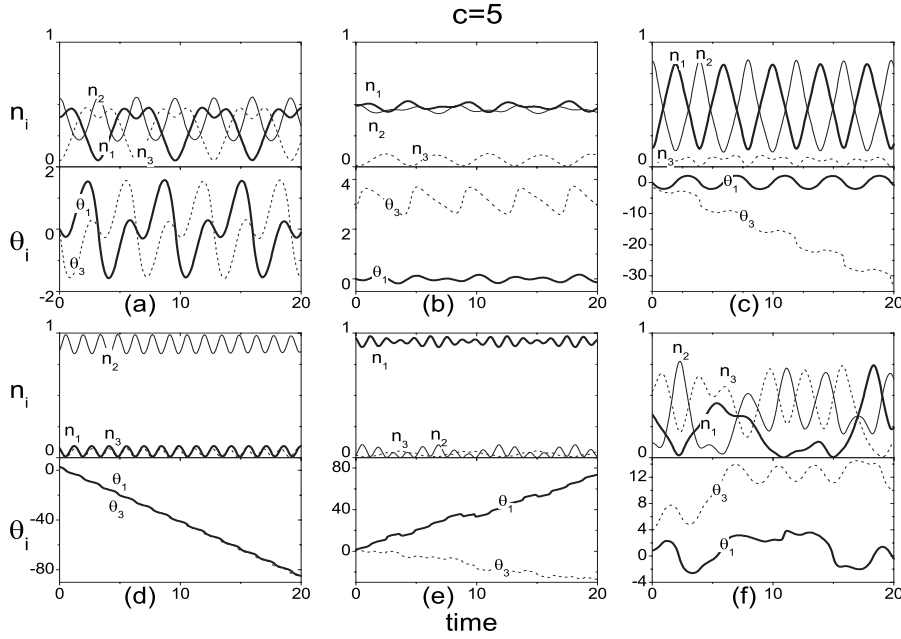$$G = vg(J_1, J_2)\sin(\theta_3) + J_1\theta_1 + J_2\theta_3, \qquad (12)$$

where

FIG. 7. The evolutions of n_1 (heavy line), n_2 (thin line), n_3 (dashed line) and θ_1 (heavy line), θ_3 (dashed line) in symmetric wells for strong interactions ($c/v=5$), with initial values (a) the same as Fig. 4, ($n_1=0.4, n_3=0.05, \theta_1=0, \theta_3=0$); (b) ($n_1=0.49, n_3=0.012, \theta_1=0, \theta_3=2.82$); (c) ($n_1=0.15, n_3=0, \theta_1=0, \theta_3=0$); (d) ($n_1=0.076, n_3=0.066, \theta_1=2.54, \theta_3=2.79$); (e) ($n_1=0.96, n_3=0.02, \theta_1=1.36, \theta_3=1.34$); (f) ($n_1=0.348, n_3=0.532, \theta_1=0.817, \theta_3=3.843$).

$$g(J_1, J_2) = \frac{v\sqrt{1-J_1-J_2}\sqrt{J_2}}{c(1-J_1-2J_2)}.$$

Then the Hamiltonian becomes

$$H' = \frac{1}{2}c(2J_1^2 + 2J_2J_1 - 2J_1 + 2J_2^2 - 2J_2 + 1)$$
$$+ v\sqrt{1-J_1-J_2}\sqrt{J_1}\cos(\Phi_1). \quad (13)$$

The new canonical variables have relations with the old canonical variables,

$$n_1 = J_1, \quad (14a)$$

$$n_3 = J_2 + v\cos(\theta_3)g(J_1, J_2), \quad (14b)$$

$$\Phi_1 = \theta_1 + v\sin(\theta_3)g^{(1,0)}(J_1, J_2), \quad (14c)$$

$$\Phi_2 = \theta_2 + v\sin(\theta_3)g^{(0,1)}(J_1, J_2). \quad (14d)$$

Since the action variable J_2 is constant, the action-angle variables J_1, Φ_1 can be solved first from the new canonical equations (14). Notice that $J_1 = n_1$ is the population in well one, and $\Phi_1 \approx \theta_1$ is the relative phase of the quantum state in well one and well two. The oscillations shown in Fig. 7(c) are the same as the zero-phase mode oscillations in a two-well trapped system.

Figures 7(d) and 7(e) show self-trapping of BECs in the middle well and self-trapping in one side well, respectively. These motions have close relations to the property of fixed points, and will be discussed in detail at the next section.

Figure 7(f) shows the chaotic trajectory, which corresponds to the chaotic region in the Poincaré section. In this case, the population in each well shows irregular oscillation with respect to time.

IV. TRANSITION TO SELF-TRAPPING

A. Self-trapping in one well

Self-trapping is caused by the nonlinear interactions. For the symmetric two-well system, as we have known, self-trapping happens only when the interaction parameter excesses a critical value. Calculating the average population for the same initial value $a_1(0)=1, a_2(0)=0$ with a different interaction strength c/v can be shown in Fig. 8(a). The Hamiltonian used for calculation is
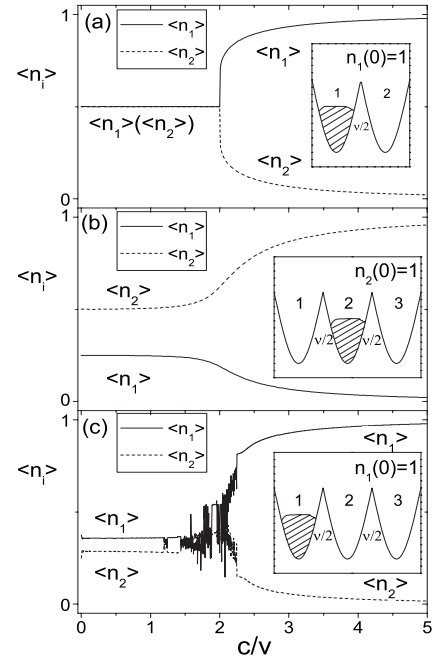

FIG. 8. The average of n_1, n_2 for different interactions c/v in the two-well system (a) and the triple-well system [(b) and (c)], with initial value (a) $n_1(0)=1$, (b) $n_2(0)=1$, (c) $n_1(0)=1$. The schematic sketch of the potential is shown in the figures.
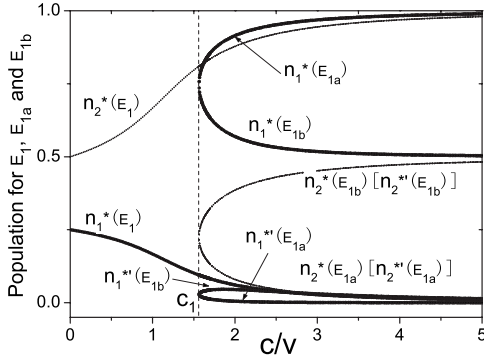
FIG. 9. The populations n_1^* (heavy line) and n_2^* (thin line) for the levels labeled by E_1, E_{1a}, and E_{1b} in Fig. 3.

$$\hat{H} = \begin{pmatrix} c|a_1|^2 & -\dfrac{v}{2} \\ -\dfrac{v}{2} & c|a_2|^2 \end{pmatrix}.$$

It is clearly shown that, when $c/v > 2$ the averaged n_1 is no longer equal to $1/2$ indicating the beginning of the self-trapping. Soon after that, with increasing the interaction, the BECs will be trapped in well one completely. Because the transition corresponds to crossing over a separatrix from oscillation to liberation, at the transition point $c/v = 2$ the scaling law follows a logarithm function [21,22].

For our triple-well system, the high-dimensional phase space permits the existence of chaos and the smooth movement of the fixed points to the boundary (the latter point will be clearly shown in Fig. 9), so we expect that the transition to self-trapping in the triple-well system will show distinguished property from that of the double-well system. To demonstrate it, we calculate the time averaged population for different interactions with the initial conditions $n_2(0) = 1$ and $n_1(0) = 1$, denoting initial BECs uploaded in the middle well and left-hand well, respectively. The results are shown in Figs. 8(b) and 8(c).

For the linear case, i.e., $c = 0$, in Fig. 8(b), substituting $(a_1 = 0, a_2 = 1, a_3 = 0)$ to Eq. (9), we can get one set of C_i,

$$C_1 = 0, \quad C_2 = -\frac{i}{\sqrt{2}}, \quad C_3 = \frac{\pi}{2}, \quad C_4 = 1, \quad C_5 = 0.$$

Then from Eq. (8) we have the averaged populations

$$\langle n_1 \rangle = \langle n_3 \rangle = |C_2|^2/2 = \frac{1}{4}, \quad \langle n_2 \rangle = |C_4|^2/2 = \frac{1}{2}.$$

Likewise, in Fig. 8(c), substituting $(a_1 = 1, a_2 = 0, a_3 = 0)$ to Eq. (9), we can get one set of C_i,

$$C_1 = \frac{1}{2}, \quad C_2 = \frac{1}{2}, \quad C_3 = 0, \quad C_4 = -\frac{i}{\sqrt{2}}, \quad C_5 = \frac{\pi}{2}.$$

From Eq. (8) we have the averaged populations

$$\langle n_2 \rangle = |C_4|^2/2 = \frac{1}{4}, \quad \langle n_1 \rangle = \langle n_3 \rangle = \frac{1 - \langle n_2 \rangle}{2} = \frac{3}{8}.$$

For the weak interaction, i.e., $c < c_1$, the averaged populations are still similar to the linear case. However, when the interaction strength is close to the critical point c_1, the averaged populations change dramatically. For Fig. 8(b), the averaged population $\langle n_2 \rangle$ increases monotonically and smoothly to unite. No scaling law is observed. This is due to the fact that in the 4D phase space the fixed point can move smoothly to the boundary without any bifurcation. For Fig. 8(c), the averaged populations become turbulent near the critical point. This is a result of chaotic trajectory in the phase space. Meanwhile, $\langle n_1 \rangle$ and $\langle n_3 \rangle$ are no longer equal. When the interaction is larger than 2.25, the averaged population $\langle n_1 \rangle$ becomes smooth and tends to unite rapidly.

For the triple-well system, when the interaction strength exceeds the critical value c_1, as mentioned before, new levels E_{1a}, E_{1b} will appear. Accordingly, new fixed points will emerge, and the phase space will tend to be divided into several subspaces around the stable fixed points. In Fig. 9 we plot populations n_1^* and n_2^* for the levels labeled by E_1, E_{1a}, and E_{1b} as a function of c/v. Corresponding to eigenenergy E_{1a} there are two eigenstates denoted by n_i^* and $n_i^{*\prime}$, respectively. The same thing happens to level E_{1b}. Recall that E_1, E_{1a} are stable levels. When the interaction is very strong, the averaged population $\langle n_2 \rangle$ of the motions of BECs uploaded initially in the middle well is close to $n_2^*(E_1)$, while $\langle n_1 \rangle$ of the motions of BECs uploaded initially in well one is close to $n_1^*(E_{1a})$, as shown in Figs. 8(b) and 8(c).

B. Self-trapping in two wells

In the above, we have investigated the self-trapping of BECs in the single well. In this part, we will investigate whether the BECs atoms can be self-trapped only in two wells.

Considering the interference, the initial relative phase should be very important, so we calculate the mean value of $\langle n_1 + n_2 \rangle$ as a function of c/v for the different phase θ_1 with the initial value $(n_1 = 0.5, n_2 = 0.5, n_3 = 0)$, and the mean value of $\langle n_1 + n_3 \rangle$ as a function of c/v for the different phases $\theta_1 - \theta_3$ with initial values $(n_1 = 0.5, n_2 = 0, n_3 = 0.5)$, respectively. The main results are shown in Fig. 10.

It is shown that, with increasing the atomic interaction, BECs will be trapped in the two wells where it is initially uploaded and the Josephson oscillation can be completely blocked. Both cases also suggest that the relative phase can dramatically influence the transition to self-trapping for BECs. In Fig. 10(a), when the relative phase is zero, the Josephson oscillation and the self-trapping can emerge alternately, whereas in the case of Fig. 10(b), the π value of the relative phase gives a robust self-trapped BEC. In both cases, we also see the occurrence of the chaos making the curves look irregular. Interestingly, the onset of chaos can also be controlled by the relative phase, e.g., the elimination of the relative phase will reduce the chaos and make the BECs safely turn from an oscillation state to a self-trapping state as shown in Fig. 10(b).
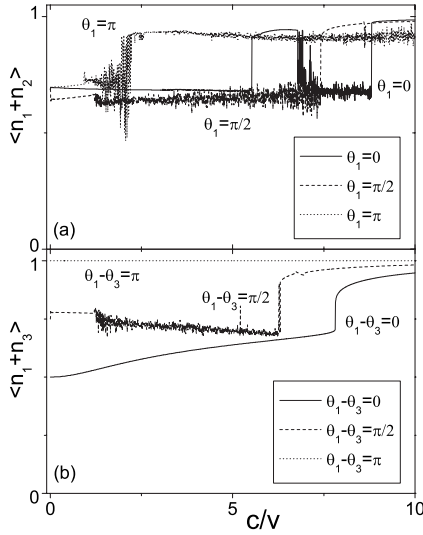
FIG. 10. The mean value of (a) $\langle n_1+n_2 \rangle$ and (b) $\langle n_1+n_3 \rangle$ with the initial value (a) ($n_1=0.5$, $n_2=0.5$, $n_3=0$), (b) ($n_1=0.5$, $n_2=0$, $n_3=0.5$) for a different relative phase.

V. TILTED TRIPLE WELL, $\gamma \neq 0$

In this section we extend the above discussions to the tilted triple-well system. In this system, the diverse type of Josephson oscillations also emerge around the eigenstates. In light of the energy spectra (Fig. 2), we can readily find out the parameter regime for different kinds of oscillations. So, we will focus on the transition to self-trapping that is of more interest. We want to see how the transition is influenced by tilting the wells.

A. Linear oscillation solutions

For the linear case, i.e., $c=0$, the system is analytically solvable, so the solutions of (a_1, a_2, a_3) are

$$a_1 = \frac{1}{2}C_4 \cos\left(\sqrt{\frac{v^2}{2}+\gamma^2}t + C_5\right) + \frac{1}{2\left(\frac{v^2}{2}+\gamma^2\right)}$$

$$\times \left[\gamma C_2 \cos\left(\sqrt{\frac{v^2}{2}+\gamma^2}t + C_3\right) + vC_1\right], \quad (15a)$$

$$a_2 = \frac{1}{\frac{v^2}{2}+\gamma^2}\left[-\frac{v}{2}C_2 \cos\left(\sqrt{\frac{v^2}{2}+\gamma^2}t + C_3\right) + \gamma C_1\right],$$

$$(15b)$$

$$a_3 = \frac{1}{2}C_4 \cos\left(\sqrt{\frac{v^2}{2}+\gamma^2}t + C_5\right) - \frac{1}{2\left(\frac{v^2}{2}+\gamma^2\right)}$$

$$\times \left[\gamma C_2 \cos\left(\sqrt{\frac{v^2}{2}+\gamma^2}t + C_3\right) + vC_1\right], \quad (15c)$$

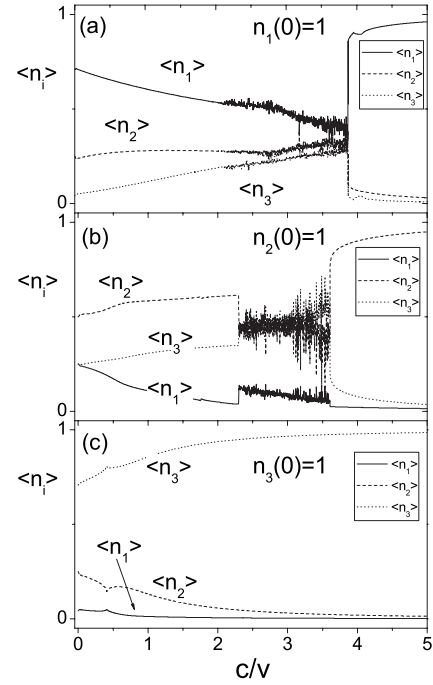where C_i are complex integral constants and like the sym-

FIG. 11. The average of n_i for different interactions c/v in asymmetric wells $\gamma=-1$ with initial value (a) $n_1(0)=1$, (b) $n_2(0)=1$, (c) $n_3(0)=1$.

metric case, are determined by initial conditions. It is clear that a_1, a_2, and a_3 vary with respect to time, periodically. The period $T=2\pi/\sqrt{\frac{v^2}{2}+\gamma^2}$.

B. Transition to self-trapping

When the interaction is strong we still observe the self-trapping of BECs in the tilted system. We plot the averaged populations in their dependence of the interaction strength with choosing parameter $\gamma=-1$ and initial conditions $n_1=1$, $n_2=1$, and $n_3=1$ in Figs. 11(a)–11(c), respectively. The schematic sketch of the wells is shown in Fig. 1(b).

For Fig. 11(a), when $c/v=0$, with the initial conditions $(a_1=1, a_2=0, a_3=0)$, we derive one set of C_i,

$$C_1 = v/2, \quad C_2 = iv/\sqrt{2}, \quad C_3 = \arccos\left(\frac{i\sqrt{2}\gamma}{v}\right),$$

$$C_4 = \frac{v}{\sqrt{v^2+2\gamma^2}}, \quad C_5 = -\arccos\left(\frac{\sqrt{v^2+2\gamma^2}}{v}\right).$$

By integrating $|a_i(t)|^2$ with respect to time and making an average over time we obtain the averaged population analytically from Eq. (15),

$$\langle n_1 \rangle = 17/24, \quad \langle n_2 \rangle = 1/4, \quad \langle n_3 \rangle = 1/24.$$

With an increase in the nonlinearity, the averaged population in well one $\langle n_1 \rangle$ decreases at first, and then becomes turbulent, indicating chaotic motions. When the interaction

parameter is larger than 3.9, the averaged population jumps up and tends to unite soon after.

In Fig. 11(b), the initial condition is $(a_1=0, a_2=1, a_3=0)$. Similarly, the averaged populations are readily obtained for the linear case, $\langle n_1 \rangle = 1/4$, $\langle n_2 \rangle = 1/2$, $\langle n_3 \rangle = 1/4$. With an increase in the nonlinearity, the averaged population $\langle n_2 \rangle$ increases smoothly at the beginning, passes a turbulence interval $[2.3, 3.6]$, and then jumps up and tends to unite. Another interesting phenomenon in the process is that the averaged population in well three is always larger than that of well one in the presence of the nonlinearity, even though in this case the zero-point energy of well three is obviously greater than that of well one. This somehow counterintuitive phenomenon is clearly the consequence of the nonlinearity.

In Fig. 11(c), when $c/v=0$, with the initial conditions $(a_1=0, a_2=0, a_3=1)$, the averaged populations have some correspondence to that of Fig. 11(a) due to behind symmetry, i.e., $\langle n_1 \rangle = 1/24$, $\langle n_2 \rangle = 1/4$, $\langle n_3 \rangle = 17/24$. With an increase in the nonlinearity, the averaged population in well three $\langle n_3 \rangle$ increases monotonically and smoothly to unite.

Comparing Fig. 11 to Fig. 8, we find that the smooth transition of the BECs in the middle well to self-trapping in the symmetric triple well is broken by tilting the wells, and lifting the well three makes BECs smoothly transit to self-trapping states without losing their stability. Figure 11 also shows that BECs in higher wells are easily self-trapped. From the above discussions, we conclude that the transition to self-trapping of the BECs in triple-well systems can be effectively controlled by tilting the wells.

VI. CONCLUSIONS

We have presented a comprehensive analysis of the tunneling dynamics for BECs in a triple-well trap both numerically and analytically. Diverse energy levels are demonstrated. Behind these unusual level structures, we reveal many new types of nonlinear Josephson oscillation. We also study the self-trapping of BECs in the one well as well as in the two well and investigate the transition from nonlinear Josephson oscillation to self-trappings. Distinguished from the double-well case, no scaling law is observed at the transition and the transition may be accompanied by an irregular regime where the motions are dominated by chaos. We also find that the transition can be effectively controlled by the relative phase between wells and tilting the wells. In the present experiments, the double well is realized in the optical traps with the use of a blue-detuned light to form a barrier. With the same technique, the triple well is also possibly realized in the optical traps. We hope our theoretical discussion will stimulate the experiments in this direction.

[1] M. H. Anderson, M. R. Matthews, C. E. Wieman, and E. A. Cornell, Science **269**, 198 (1995); K. B. Davis, M.-O. Mewes, M. R. Andrews, N. J. van Druten, D. S. Durfee, D. M. Kurn, and W. Ketterle, Phys. Rev. Lett. **75**, 3969 (1995); C. C. Bradley, C. A. Sackett, J. J. Tollett, and R. G. Hulet, *ibid.* **75**, 1687 (1995).

[2] L. Pitaevskii and S. Stringari, Bose-Einstein Condensation (Oxford University Press, Oxford, 2003).

[3] A. Smerzi, S. Fantoni, S. Giovanazzi, and S. R. Shenoy, Phys. Rev. Lett. **79**, 4950 (1997); G. J. Milburn, J. Corney, E. M. Wright, and D. F. Walls, Phys. Rev. A **55**, 4318 (1997).

[4] Biao Wu and Qian Niu, Phys. Rev. A **61**, 023402 (2000); O. Zobay and B. M. Garraway, *ibid.* **61**, 033603 (2000); R. D'Agosta and C. Presilla, *ibid.* **65**, 043609 (2002).

[5] M. Holthaus, Phys. Rev. A **64**, 011601(R) (2001).

[6] S. Raghavan, A. Smerzi, S. Fantoni, and S. R. Shenoy, Phys. Rev. A **59**, 620 (1999).

[7] J. Liu, L. Fu, B. Ou, S. Chen, D. Choi, B. Wu, and Q. Niu, Phys. Rev. A **66**, 023404 (2002).

[8] Anthony J. Leggett, Rev. Mod. Phys. **73**, 307 (2001), and references therein.

[9] D. Witthaut, E. M. Graefe, and H. J. Korsch, Phys. Rev. A **73**, 063609 (2006); Biao Wu and Jie Liu, Phys. Rev. Lett. **96**, 020405 (2006).

[10] L. D. Landau and E. M. Lifshitz, Quantum Mechanics (Pergamon Press, New York, 1997).

[11] Michael Albiez, R. Gati, Jonas Fölling, S. Hunsmann, M. Cristiani, and M. K. Oberthaler, Phys. Rev. Lett. **95**, 010402 (2005).

[12] Roberto Franzosi and Vittorio Penna, Phys. Rev. A **65**, 013601 (2001).

[13] Roberto Franzosi and Vittorio Penna, Phys. Rev. E **67**, 046227 (2003).

[14] P. Buonsante, R. Franzosi, and V. Penna, Phys. Rev. Lett. **90**, 050404 (2003).

[15] The triple-well system differs from the trimer-train system in that the periodic boundary condition is eliminated. This difference is essential both in mathematics and physics. See, for example, E. M. Graefe, H. J. Korsch, and D. Witthaut, Phys. Rev. A **73**, 013617 (2006); S. Mossmann and C. Jung, *ibid.* **74**, 033601 (2006).

[16] The "self-trapping" of BECs in optical lattice has been observed experimentally. However, the behind physics is not fully understood. Refer to T. Anker, M. Albiez, R. Gati, S. Hunsmann, B. Eiermann, A. Trombettoni, and M. K. Oberthaler, Phys. Rev. Lett. **94**, 020403 (2005); Tristram J. Alexander, Elena A. Ostrovskaya, and Yuri S. Kivshar, *ibid.* **96**, 040401 (2006); Roberto Livi, Roberto Franzosi, and Gian-Luca Oppo, *ibid.* **97**, 060401 (2006); Bingbing Wang, Panming Fu, Jie Liu, and Biao Wu, Phys. Rev. A **74**, 063610 (2006).

[17] A. J. Lichtenberg and M. A. Lieberman, *Regular and Stochastic Motion* (Springer-Verlag, New York, 1983); L. E. Reichl, *The Transition to Chaos* (Springer-Verlag, New York, 1992).

[18] Jie Liu, Biao Wu, and Qian Niu, Phys. Rev. Lett. **90**, 170404 (2003).

[19] An introduction of MATHEMATICA could be found from http://www.wolfram.com/

[20] Jie Liu, Chuanwei Zhang, Mark G. Raizen, and Qian Niu, Phys. Rev. A **73**, 013601 (2006); Chuanwei Zhang, Jie Liu, Mark G. Raizen, and Qian Niu, Phys. Rev. Lett. **92**, 054101 (2004).

[21] Guan-Fang Wang, Li-Bin Fu, and Jie Liu, Phys. Rev. A **73**, 013619 (2006).

[22] Li-Bin Fu and Jie Liu, Phys. Rev. A **74**, 063614 (2006).